

18. GEOCHEMISTRY AND PETROLOGY OF PLEISTOCENE ASH LAYERS ERUPTED AT LAS CAÑADAS EDIFICE (TENERIFE)¹

Uta Rodehorst,^{2,3} Hans-Ulrich Schmincke,² and Mari Sumita²

ABSTRACT

Sixty-eight fallout trachytic to phonolitic ash layers recovered from Sites 953, 954, and 956 during Leg 157 are interpreted as a result of explosive eruptions of the Las Cañadas edifice on Tenerife. Their biostratigraphic ages range from 0.3 to 3.8 Ma. Tephra layers consist dominantly of highly vesicular pumice and 1–10 vol% phenocrysts. Alkali feldspar occurs in almost all layers; but plagioclase, clinopyroxene, amphibole, phlogopite, sphene, Fe-Ti oxides, and hauyne appear in some. Nepheline, hauyne and sodalite occur together in one of the younger (0.4 Ma) layers at Site 953 (Sample 157-953A-2H-5, 148–150 cm). The chemical composition of glass shards, analyzed by electron microprobe in 20 samples changes from trachytic to phonolitic in the time interval between 2 and 0.4 Ma. The concentration of trace elements (Ce, La, Mn, Fe, and Zr) in sphene, analyzed in four layers, is variable. Bulk ash analyses by X-ray fluorescence and inductive coupled plasma mass spectrometry show similar major and trace element patterns for all tephra layers. Although eruptive gaps have been postulated from distribution of volcanic rocks on land, the stratigraphic distribution of submarine ash layers suggests that explosive volcanic activity of the Cañadas volcano on Tenerife was fairly continuous. None of the noneruptive hiatuses postulated between 0.37 and 0.65 Ma, 0.85 and 1.2 Ma and 1.6 and 2.0 Ma in the Cañadas series on land were confirmed. Apparently fallout ash layers in the marine environment provide a more reliable record of volcanic activity on land.

INTRODUCTION

Pico de Teide (3718 meters above sea level [masl]), the third highest oceanic volcano on Earth, is arguably the most explosive one. Compared with its two mighty counterparts, Mauna Loa (4170 masl) and Mauna Kea (4206 masl) on the island of Hawaii, both of which are basaltic in composition, the volcanic rocks of the Las Cañadas edifice are almost entirely composed of lavas and pyroclastics of evolved phonolitic to trachyphonolitic composition. The cone of Pico de Teide rises ~1700 m from a caldera whose present bottom is at ~2000 masl and whose semicircular walls rise up to 600 m. Pico de Teide itself appears to be composed mostly of basalts covered by a thin layer of basaltic lavas. The caldera walls are composed largely of lavas, minor amounts of ignimbrites, and fallout tephra layers whose age ranges from ~3 Ma at the discontinuously exposed Lower Group at the base to ~0.18 Ma at the Diego Hernandez Formation in the northeastern part of the caldera wall (Ancochea et al., 1990; Marti et al., 1989, 1994). The caldera wall, which is visible for 27 km, provides almost continuous outcrop of the precaldera rocks. Our aim in drilling tephra layers from Tenerife during Ocean Drilling Program (ODP) Leg 157 was to find answers to the following questions:

1. When did explosive activity of the Las Cañadas edifice, Pico de Teide, and its older neighbor Pico Viejo begin?
2. Was explosive activity during the evolution of Cañadas volcano continuous or discontinuous?
3. Can tephra layers from Deep Sea Drilling Project (DSDP) Site 397 be correlated with those from Sites 955 and 956?
4. Do the tephra layers record the mineralogical and geochemical evolution of the Las Cañadas edifice and Pico de Teide?

5. Can the temporal, chemical, and petrological evolution reflected by the tephra layers be correlated with that of corresponding deposits on land?

Tephra fallout layers in marine sediments are especially suitable for reconstructing the petrologic evolution of volcano-magma systems (e.g., Paterne et al., 1988; Dehn et al., 1991; Straub, 1995; Fisher and Schmincke, 1984). Tephra layers deposited on land are more rapidly eroded and, as in the case of Tenerife, are covered by younger tephra or lava flows. Many lower Pliocene and Pleistocene tephra layers related to the growth and evolution of the Las Cañadas edifice were recovered at Sites 953 through 956 and studied with sedimentologic, geochemical, and petrologic methods. These tephra layers consist dominantly of highly evolved ashes and lapilli younger than 3.8 Ma and older than 0.3 Ma. Hole 955A, 211 km east of Tenerife, will not be discussed as only one significant tephra layer has been sampled. Here we present preliminary data on the volcanic and petrologic evolution of this large volcanic complex. Basaltic glasses in some of these layers (sideromelane) are discussed in a companion paper (Gurenko and Schmincke, Chap. 25, this volume).

METHODS

Sample Preparation

The tephra samples were shock-frozen and then sieved through 63-, 125-, and 250- μ m polyester screens and 500- μ m, 1-mm, 2-mm sieves with distilled water and dried at 40°C. The altered and lithified samples, and the so-called beach sands that mostly contain skeletal debris from shallow water zones, were excluded. The clean pumice and phenocrysts with a grain size between 250 and 500 μ m were embedded in resin, and 20 polished sections were prepared for electron microprobe analysis and microscopic study.

Electron Microprobe

Electron microprobe analyses were performed on a CAMECA SX 50 microprobe equipped with four spectrometers at GEOMAR, Kiel.

¹Weaver, P.P.E., Schmincke, H.-U., Firth, J.V., and Duffield, W. (Eds.), 1998. *Proc. ODP, Sci. Results, 157*: College Station, TX (Ocean Drilling Program).

²GEOMAR Forschungszentrum, Wischhofstrasse 1-3, D-24148 Kiel, Federal Republic of Germany.

³Present address: Mineralogisch-Petrographisches Institut, Universität Kiel, Olshausenstr. 40, 24118 Kiel, Federal Republic of Germany. ur@min.uni-kiel.de

Analytical conditions were 15 kV accelerating voltage and 12 nA sample current for glass and hauyne, 20 nA for feldspar, amphibole, phlogopite, and sphene, and 30 nA for olivine and clinopyroxene. In alkali-rich minerals, sodium and potassium were among the first elements analyzed. Sphene is rich in rare earth and other trace elements (light rare earth to >1 wt%, for example, Ce_2O_3 as much as 1.8 wt%), which can be measured by microprobe. Synthetic standards (P&H Developments) for rare earth elements (REE) with 4 wt% element concentrations were used. To avoid the problem that many L-alpha lines of the different REE undergo (i.e., interference from other X-ray lines), only La, Nd, and Ce were analyzed because these have strong lines and clear peaks. In sphene, the REE and Mn substitute for Ca, whereas Fe, Al, Zr, V, and Nb substitute for Ti (Oberti et al., 1991). The elements Ce, La, Nd, Mn, and Fe were measured in sphene from four different ash layers. The standard errors (deviation from expected standard value and the measured average of the standard during several analyses) were Ce: 2.7%; La: 1.5%; Nd: 3.9%; Mn: 2.4%; and Fe: 0.5%.

Bulk Chemistry

X-ray fluorescence (XRF) analyses were carried out on clean pumice separates of eight samples where there was sufficient sample material and no visible phenocrysts. We also analyzed one crystal-rich sample with basaltic mineralogy (Sample 157-954A-7H-4, 59–61 cm). Inductively coupled plasma mass spectrometry (ICP-MS) analyses of 35 trace elements were performed on three phenocryst-free pumice samples.

Geochronology

Alkali feldspar and plagioclase crystals were separated for single crystal dating. The grain size of the crystals was between 500 and 200 μm . The $^{40}\text{Ar}/^{39}\text{Ar}$ single crystal laser ages are discussed in a separate paper (Bogaard, Chap. 19, this volume).

ANALYTICAL RESULTS

Core Descriptions

All felsic fallout tephra layers of upper Pliocene/Pleistocene age are assumed to have erupted from the Las Cañadas edifice on Tenerife, based on their bio- and magnetostratigraphic ages, ranging from >3.8 to 0.3 Ma (Brunner et al., Chap. 9, this volume). During this time interval, no volcanic activity (La Gomera) or almost exclusively mafic activity is recorded from the other Canary Islands (Lanzarote, Fuerteventura, La Palma, and Gran Canaria; Coello et al. 1992). The ages of the phonolithic tephra layers in Barranco de Guadeque (Gran Canaria), whose age maybe between 3 and 2 Ma are presently being determined.

The combined total thickness of all Pliocene/Pleistocene felsic volcanoclastic layers in Hole 956A is ~250 cm (26 tephra layers), in Holes 954A and 954B ~170 cm (35 tephra layers), and in Hole 953A ~52 cm (nine tephra layers). Felsic tephra layers occur down to 122 meters below seafloor (mbsf; Hole 953A), 140 mbsf (Holes 954A, 954B), 118 mbsf (Hole 955A) and 100 mbsf (Hole 956A), respectively. Below 110 mbsf, the core recovery at Hole 954B was only ~50%, and no sediments ranging in age from 1 to 2.5 Ma are present in Hole 954B. Most likely, the number of ash layers is much higher at this locality being close to Tenerife. In summary, the bulk of the ash evidently was transported to the northeast to Sites 954 and 953 as few ash layers occur at Site 956 southeast of the island even though this Site is closer to Tenerife (Fig. 1). Table 1 summarizes biostratigraphic age (Brunner et al., Chap. 9, this volume), macroscopic descriptive information for all samples (Schmincke, Weaver, Firth, et al., 1995), and median and sorting. The tephra layers contain pumice as a main component next to glass shards, lithic fragments, microlites and 1–10 vol% phenocrysts. These constituents are mixed with variable amounts of nanofossil

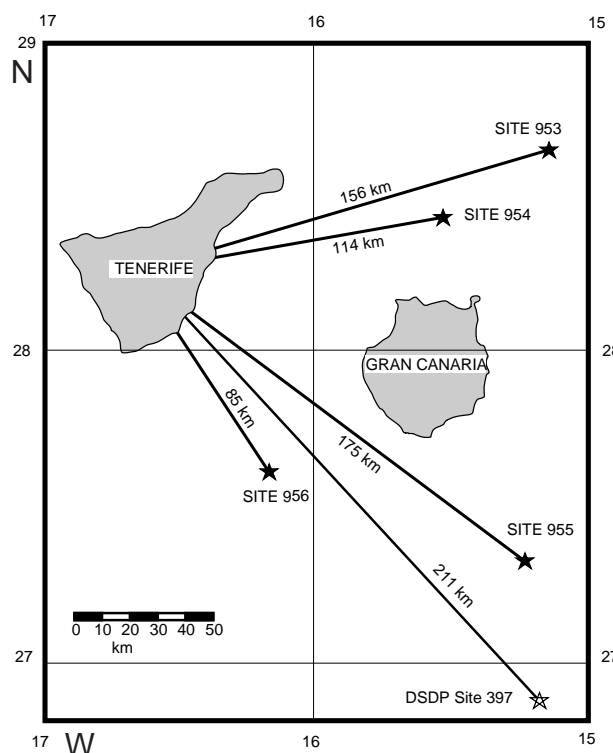


Figure 1. Locations of drill sites around Gran Canaria, showing distances to the approximate center of the Las Cañadas caldera on Tenerife.

mud, foraminifers and skeletal debris. The most common phenocryst is alkali feldspar. Plagioclase, amphibole, biotite, sphene, hauyne, sodalite, pyroxene, nepheline, and Fe-Ti-oxides occur in minor amounts. The pumice is fresh, except in the deeper cores from Hole 954 (Samples 157-954B-7R-2, 22–25 cm, and 12R-1, 92–93 cm) and Hole 956 (Sample 157-956A-11H-5, 125–127 cm). Some more strongly altered layers occur in Hole 956 (Sample 157-956A-3H-5, 100–112 cm; Table 1). To compare Sites 953, 954, and 956 with observations made on land, biostratigraphic ages (Schmincke, Weaver, Firth, et al., 1995) have been plotted together with the K/Ar and $^{40}\text{Ar}/^{39}\text{Ar}$ ages from the caldera wall (Marti et al., 1994; Fig. 2).

Phenocryst Composition

Pumice and phenocrysts of feldspar, phlogopite, amphibole, pyroxene, olivine, hauyne, and sphene were analyzed by microprobe in 20 polished thin sections. The oldest analyzed samples are from Hole 956A (1.6–2 Ma). The samples studied from Hole 954A range between 0.43 and 1 Ma, those of Hole 953A from 0.38 and 0.7 Ma. One layer sampled in Hole 953A is 1 Ma (Sample 157-953A-7H-3, 70–72 cm) and another is 1.55 Ma (Sample 157-953A-11H-5, 39–40 cm). The mineral abundance for the three sites vs. age is illustrated in Figure 3.

Alkali feldspars was analysed in seven thin sections (Fig. 4) and do not vary in composition with time. Two primary fallout ashes from Tenerife (Samples 157-953A-2H-4, 77–79 cm, and 157-954A-9H-2, 145–147 cm) are characterized by plagioclase. Two samples from Hole 956 (Samples 157-956A-7H-6, 70–76 cm, and 6H-2, 124–124 cm) contain plagioclase and olivine. The related pumices are rounded, and sorting is low, which indicate reworking.

Hauyne occurs in ~30% of the tephra layers, mostly in the younger tephra (<0.65 Ma) and in tephra older than 1.7 Ma. Sample 157-953A-2H-5 (148–150 cm) contains nepheline, sodalite, and hauyne.

Table 1. List of samples, grain size analyses, and macroscopic descriptions.*

Label	Core, section, interval (cm)	Depth	Biostrat. age (Ma)	Stderr. age	Sorting	Median (μm)	Thickness (cm)	Notes	Deposition	Color
157-953A-										
URO-3-1	1H-5, 122-124	7.22	0.30	0.08	0.625	88	73	Mixed sediment		Dark gray
URO-3-2	2H-4, 77-79	12.87	0.38	—	—	—	15	—	s	Dark brown
URO-3-3	5H-1, 148-150	15.08	0.41	—	—	—	10	Pumice sand	p	Gray
URO-3-4	3H-6, 143-144	26.03	0.56	—	—	—	—	—		—
URO-3-5	4H-1, 71-72	27.31	0.57	—	—	—	8	Dark crystal vitric ash		Dark gray
URO-3-6	5H-1, 54-56	36.64	—	—	—	—	—	—	p ?	Dark green
URO-3-7	5H-1, 56-57	36.66	0.70	—	1.650	51	4	—	p ?	Light green
URO-3-8	5H-1, 57-58	36.67	—	—	—	—	—	—	p ?	Light green
URO-3-9	7H-3, 70-72	58.80	1.00	—	1.900	38	2.5	Homogeneous fine volcanic ash	p ?	Medium brown
URO-3-10	11H-5, 39-40	99.49	1.55	—	2.025	44	8	Disperse ash layer	p	Yellow green
URO-3-11	12H-6, 54-55	110.64	1.70	—	2.000	31	2	—		—
URO-3-12	14H-1, 83-84	122.43	1.86	—	1.850	134	2	Disperse ash layer		—
157-954A-										
URO-4-1	3H-1, 88-89	11.38	0.30	0.04	1.500	26	5	—	p	Dark olive green
URO-4-2	3H-1, 132-133	11.82	0.30	—	—	—	40	—		Dark brown
URO-4-3	3H-2, 92-93	12.92	0.31	—	1.500	74	9	—		Light brown brown
URO-4-4	3H-2, 110-111	13.10	0.32	—	—	—	—	—		Light brown
URO-4-5	3H-6, 139-145	19.39	0.39	—	1.250	274	—	Pumice sand with granule pumice clasts	s	—
URO-4-6	4H-3, 43-44	23.43	0.43	—	—	—	—	—		Gray green
URO-4-7	4H-6, 87-88	28.37	0.49	—	1.750	36	0.5	—		Light green
URO-4-8	4H-6, 120-122	28.70	0.49	—	0.900	177	—	—		—
URO-4-9	6H-5, 58-60	45.58	0.68	—	1.750	37	—	—		—
URO-4-10	6H-5, 67-69	45.67	—	—	2.500	31	—	—		—
URO-4-11	6H-5, 71-73	45.71	0.68	—	1.750	53	10	—		—
URO-4-12	6H-5, 75-77	45.75	—	—	2.250	44	—	Coarse ash	p	Light green
URO-4-13	7H-1, 14-16	48.64	0.71	—	—	—	—	—		—
URO-4-14	7H-1, 39-41	48.89	0.72	—	2.300	31	—	—		—
URO-4-15	7H-1, 81-85	49.31	0.72	—	2.200	31	7.5	—		Green gray
URO-4-16	7H-2, 30-32	50.30	0.73	—	—	—	2	—		Dark gray brown
URO-4-17	7H-4, 59-61	53.59	0.77	—	0.625	149	7	Dark basalt sands		Dark gray brown
URO-4-18	8H-1, 114-116	59.14	0.83	—	1.550	22	—	Disturbed clay		—
URO-4-19	8H-2, 52-54	60.02	0.84	—	2.625	134	—	—		—
URO-4-20	8H-2, 88-90	60.38	0.84	—	2.275	19	1	Pumice sand	p ?	Gray
URO-4-21	8H-4, 61-63	63.11	0.88	—	—	—	1	Volcanic ash	p ?	—
URO-4-22	8H-7, 11-13	67.11	0.92	—	1.900	31	1.5	Volcanic ash	p ?	Green gray
URO-4-23	9H-1, 139-140	68.89	0.94	—	0.700	109	6	Interbeds		—
URO-4-24	9H-2, 140-141	70.40	0.96	—	2.050	36	—	—		Green gray
URO-4-25	9H-2, 143-144	70.43	0.96	—	1.850	31	—	—		Green gray
URO-4-26	9H-2, 145-147	70.45	0.96	—	2.025	37	6.5	—		Green gray
URO-4-27	9H-3, 7-8	70.57	0.96	—	1.900	27	1	—		Green gray
URO-4-28	9H-3, 140-141	71.90	0.97	—	0.950	102	5	Dark basaltic sand		Black
URO-4-29	9H-4, 33-34	72.33	0.98	—	1.700	250	17	Pumice		—
157-954R-										
URO-4-30	4R-1, 123-125	110.93	2.60	0.07	1.750	22	24	Vitric fine ash		Gray
URO-4-31	4R-1, 136-138	111.06	2.60	—	1.800	19	—	—		Light gray
URO-4-32	4R-2, 4-6	111.24	2.61	—	1.900	18	—	—		Light gray
URO-4-33	4R-2, 35-37	111.55	2.61	—	1.850	354	19	—	p	Gray
URO-4-34	4R-2, 89-91	112.09	2.62	—	1.800	25	4	Mixed sediment with vitric ash		Green gray
URO-4-35	5R-3, 45-47	122.75	2.79	—	2.100	24	1	—		—
URO-4-36	5R-3, 71-73	123.01	2.79	—	—	—	1	Coarse ash layer		—
URO-4-37	6R-4, 133-135	134.83	2.97	—	—	—	2	—		Yellow green
URO-4-38	7R-2, 22-25	140.32	3.06	—	—	—	—	Zeolized tuff		Gray
URO-4-39	12R-1, 92-93	187.82	3.79	0.23	—	—	—	Claystone		—
157-956A-										
URO-6-1	3H-3, 86-92	19.46	0.58	—	—	—	—	Beach sand	s	Gray
URO-6-2	3H-5, 23-29	21.83	0.67	—	—	—	—	Beach sand	s	Gray
URO-6-3	3H-5, 100-106	22.60	0.72	—	—	—	—	Palagonitic ash		Dark orange brown
URO-6-4	3H-5, 108-109	22.68	0.72	—	—	—	—	Palagonitic ash		Dark orange brown
URO-6-5	3H-5, 111-112	22.71	0.72	—	—	—	40	Palagonitic ash		Dark orange brown
URO-6-6	4H-7, 1-3	34.11	1.12	—	—	—	3	Pumice clasts from 0-3 cm		Gray
URO-6-7	5H-4, 85-86	39.95	1.34	—	—	—	—	Pumice lithic sand	s	Pale gray
URO-6-8	5H-4, 92-94	40.02	1.34	—	—	—	—	Pumice lithic sand	s	Pale gray
URO-6-9	5H-4, 118-132	41.78	1.40	—	—	—	6.5	Massive pumice sand		Black gray banded
URO-6-10	6H-2, 120-122	46.80	1.56	—	—	22	5	Pumice sand		Gray
URO-6-11	6H-2, 122-124	46.82	1.56	—	2.750	38	2	Pumice sand		Gray
URO-6-12	6H-2, 124-126	46.84	1.56	—	2.125	54	0.5	Pumice sand	s	Gray
URO-6-13	6H-2, 128-130	46.88	1.56	—	1.550	18	—	Vitric silt		Gray
URO-6-14	7H-1, 135-137	54.95	1.80	—	2.225	10	1.5	Crystal sand with pumice		Dark gray
URO-6-15	7H-2, 84-86	55.94	1.83	—	2.125	36	1	—		—
URO-6-16	7H-3, 56-58	57.16	1.87	—	—	—	6	Volcanic glass		—
URO-6-17	7H-5, 105-107	60.65	1.96	—	1.500	13	5	Pumice sand		Dark green gray
URO-6-19	7H-5, 107-109	60.67	1.96	—	—	—	4	Pumice sand		Dark green gray
URO-6-18	7H-6, 70-76	61.80	1.99	—	—	—	65	Coarse sand	s	Speckled gray
URO-6-20	7H-CC, 7-9	63.23	2.04	—	2.250	22	6	Pumice sand		Dark gray
URO-6-21	7H-CC, 11-13	63.27	2.04	—	1.950	63	1	Pumice sand		dark gray
URO-6-22	8H-5, 72-74	69.82	2.21	—	3.000	44	5	Foram pumice fine sand		—
URO-6-23	8H-5, 144-146	70.54	2.22	—	2.750	44	17	Foram pumice		Gray
URO-6-24	9H-1, 33-34	72.93	2.27	—	—	—	2.5	—		Green gray
URO-6-25	9H-1, 38-39	72.98	2.27	—	2.150	36	0.5	—		Green gray
URO-6-26	9H-1, 63-64	73.23	2.27	—	—	—	2	Coarse rounded pumice sand	s	Dark gray
URO-6-27	9H-2, 22-27	74.32	2.29	—	2.350	354	30	Lithic pumice sand, rounded	s	—
URO-6-28	9H-2, 90-92	75.00	2.33	—	1.675	77	8	Vitric silt	p	Dark green
URO-6-29	9H-3, 15-21	75.75	2.33	—	—	—	14	Pumice sand	p	Gray green
URO-6-30	9H-3, 106-107	76.66	—	—	0.625	88	—	—		—
URO-6-31	9H-3, 107-108	76.67	2.35	—	0.575	88	9	Volcanic ash	p	Green gray
URO-6-32	9H-3, 111-113	76.71	—	—	1.650	41	—	—		—

Table 1 (continued).

Label	Core, section, interval (cm)	Depth	Biostrat. age (Ma)	Stderr. age	Sorting	Median (µm)	Thickness (cm)	Notes	Deposition	Color
URO-6-33	11H-2, 68-70	93.78	2.69	—	—	—	1	Volcanic ash		Green gray
URO-6-34	11H-2, 110-113	94.20	—	—	—	—	—			—
URO-6-35	11H-2, 113-114	94.23	2.70	—	—	—	6	Pumice lapilli		—
URO-6-36	11H-2, 114-115	94.24	—	—	1.850	22	—			—
URO-6-37	11H-5, 125-127	98.85	2.77	—	1.775	36	10	—		—

Notes: * = from Schmincke, Weaver, Firth, et al. (1995). Biostrat. age = biostratigraphic age, and Stderr. = standard error (Brunner et al., Chap. 9, this volume). — = no data determined, s = secondary, and p = primary.

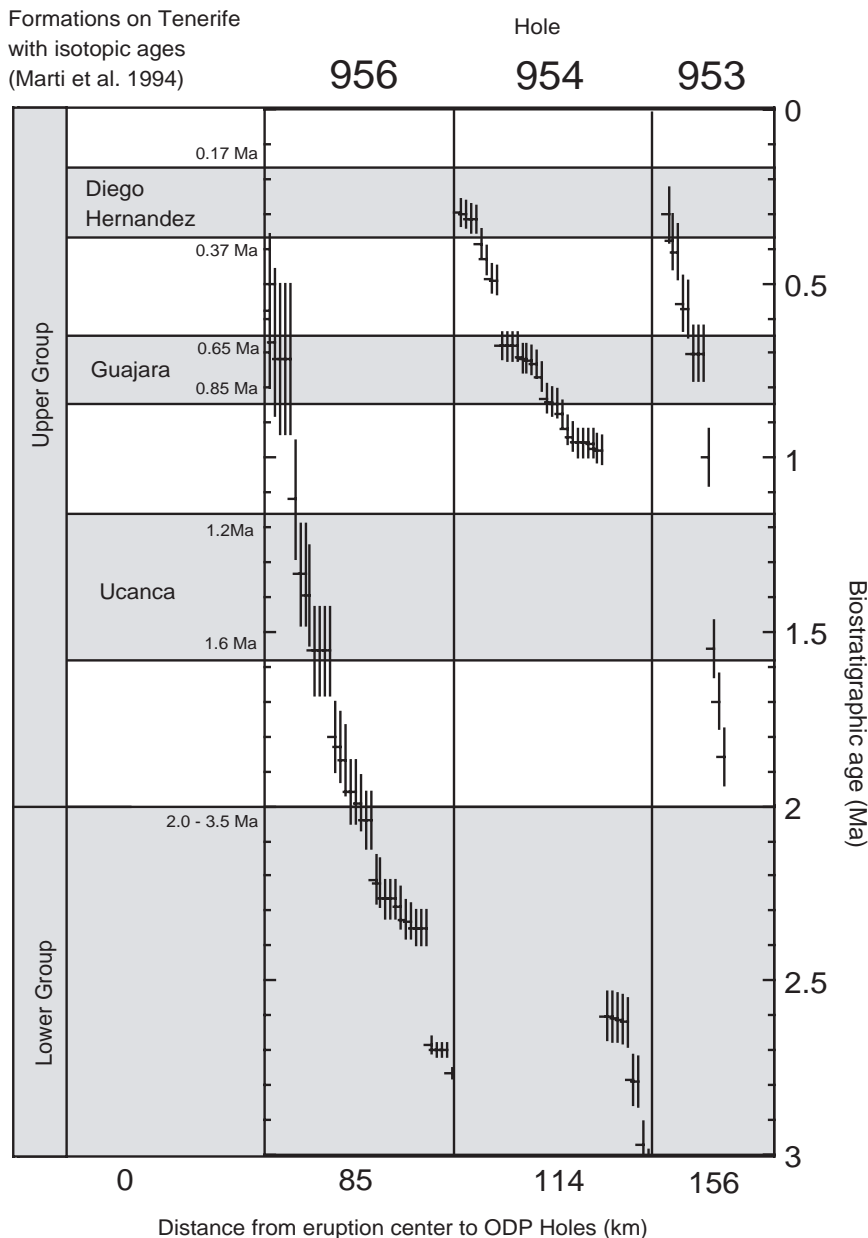


Figure 2. Biostratigraphic ages with standard deviations for Sites 953, 954, and 956 (Brunner et al., Chap. 9, this volume) compared with the ages of the units in the caldera wall (Marti et al., 1994), which were determined by ⁴⁰Ar/³⁹Ar and K-Ar age dating.

Sphene is common in the submarine ash layers from Tenerife. Sphene of Sample 157-953A-14H-1 (83–84 cm) differs chemically to the three other layers (Fig. 5). The amount of Ce, Nd, and La is low, and the Ti content varies with each sphene grain correlating with the Fe content. The three other samples substitute REE on Ca position in various amounts. An increase in the concentration of La, Ce, Fe, and Mn with increasing age is shown for these layers (Fig. 5).

Chemical Composition of Glass Shards

The composition of glass shards was analyzed in 20 samples from 2 to 0.4 Ma. Up to 20 analyses were performed for each grain mount. Representative data are listed in Table 2, and the results are plotted in Figures 6 and 7. The data were normalized volatile-free to 100%. The totals show no significant age dependence and the same trends (in-

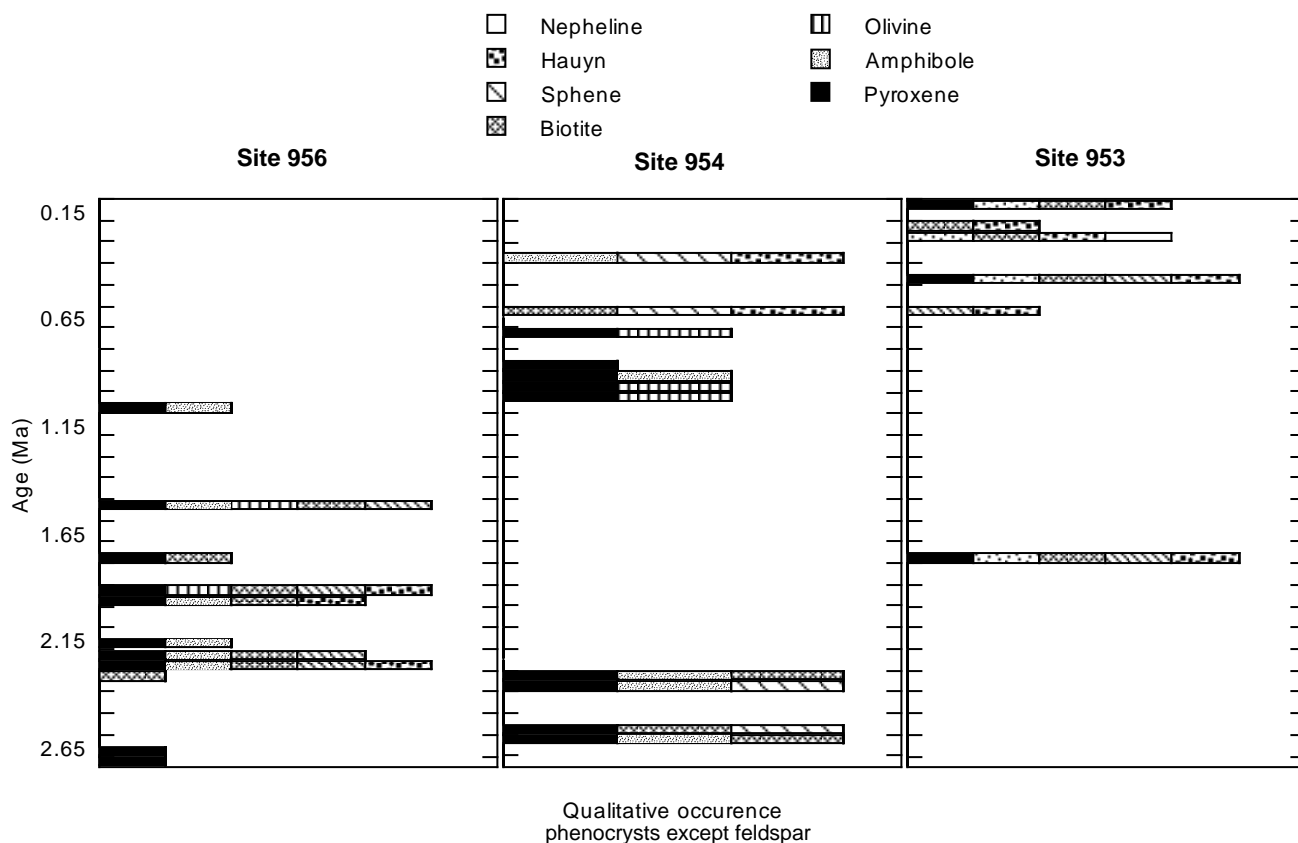


Figure 3. Mineral distribution vs. age of tephra layers from Sites 953, 954, and 956. Alkali feldspar is not shown, occurring in almost all samples. No quantitative estimation is shown, because estimation is based on the thin sections with different grain-sized fractions. One bar represents whether one sort of mineral occurs.

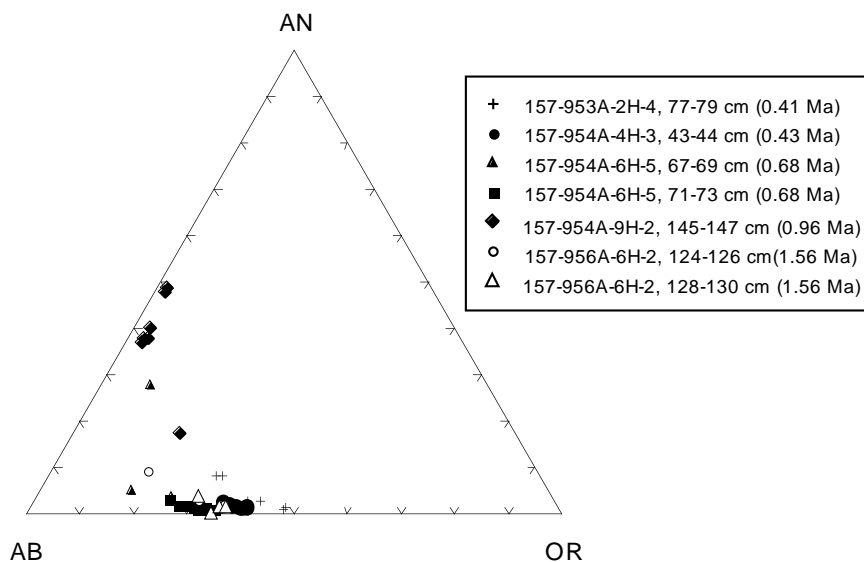


Figure 4. Feldspar compositions from individual layers, measured by electron microprobe. Each symbol corresponds to the average of 10–20 spots of a single feldspar grain.

creasing total alkalis with decreasing age) as the raw data (Fig. 8). This suggests that errors because of normalization and thus hydration should be minor. The submarine ashes are trachytic and phonolitic. Trachyandesitic glass is rare: (1) two grains in Sample 157-954A-6H-5, 67–69 cm, that were taken from the top of a 10-cm-thick layer (10–14 measurement points for each grain); (2) glass from Sample 157-953A-11H-5, 39–40 cm; and (3) one pumice grain from the

ash Sample 157-956A-6H-2, 124–126 cm, which is probably reworked.

The composition of the glasses changes with time from trachyte to phonolite (Fig. 6). Al_2O_3 decreases with increasing SiO_2 ; the FeO_{total} and MnO contents are low and show no significant trends vs. SiO_2 (Fig. 7). The glass analyses from ash Sample 157-953A-2H-4 (77–79 cm), ranging from phonolitic to basaltic within a single grain, suggest

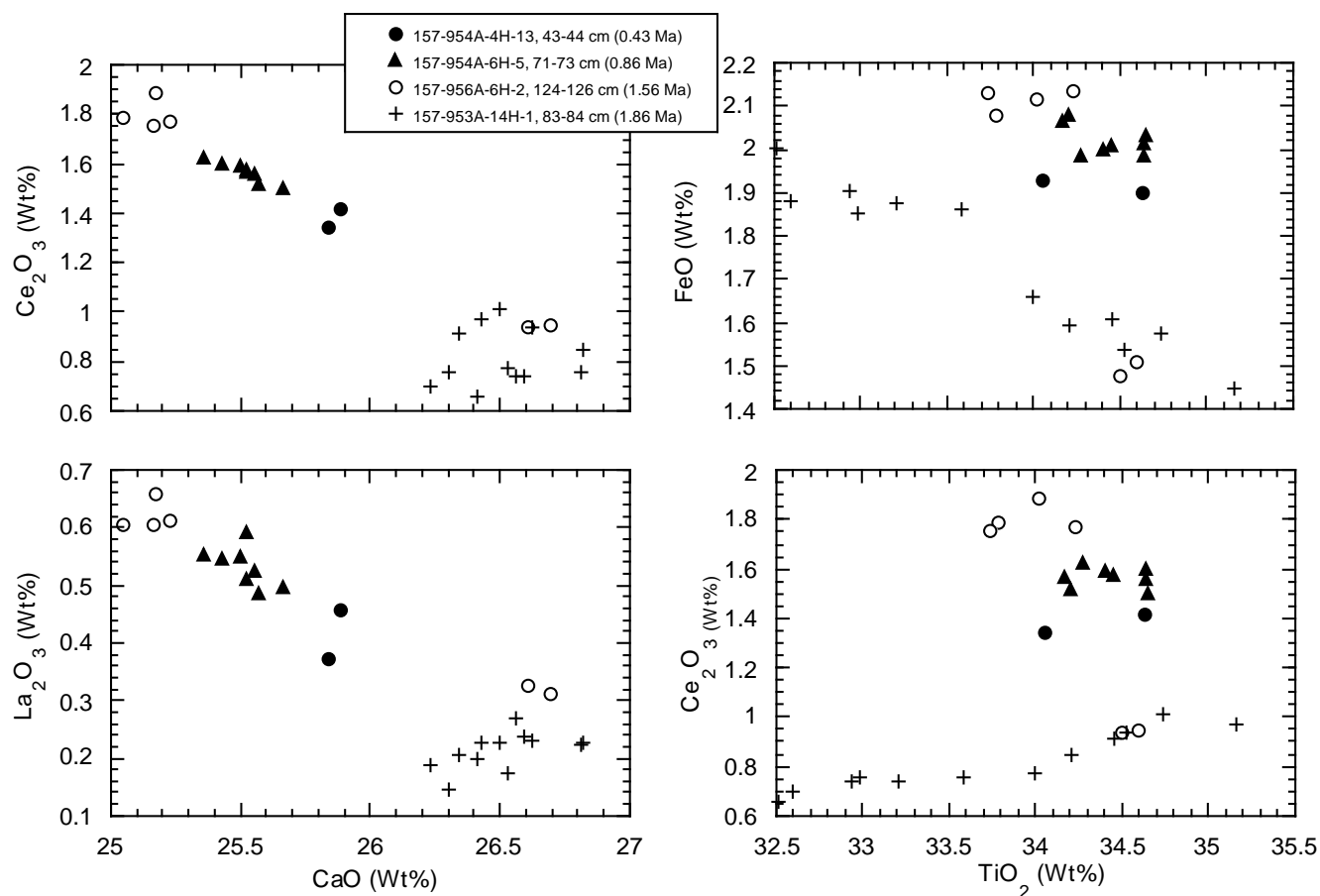


Figure 5. Microprobe analyses of sphene. Each data point corresponds to the average of 10 to 20 spots measured on one grain. The plots of Ce_2O_3 and La_2O_3 vs. CaO represent the isomorphous substitution of Ce and La on Ca position correlating well in contrast to Ce_2O_3 vs. TiO_2 , suggesting no exchange. Sphene of Sample 157-953A-14H-1, 83–84 cm (1.86 Ma), varies strongly in Ti content and substitutes lower amounts of REEs compared to the other samples.

magma mixing (Fig 9). This is confirmed by the occurrence of plagioclase and olivine phenocrysts. Magma mixing is not unusual on Tenerife as discussed by Wolff (1985) and Wolff et al. (1990).

Trace Element Composition of Glass Shards

The results of the XRF and ICP-MS analyses are listed in Tables 3 and 4. The trace element concentrations of analyzed pumice were normalized against OIB (Sun and McDonough, 1989). All samples show similar concentrations and distribution patterns (Fig. 10). Differences are not age dependent. The glasses are strongly depleted in Sr, Ba, P, Ti, and Sc which is interpreted as being caused by fractionation of feldspar, apatite, sphene and/or Fe-Ti oxides, and pyroxene in different amounts. Sample 954A-7H-4, 59–61 cm (0.77 Ma), represents one of the two basaltic tephra layers. The trace element analyses and the similarity in the enrichment patterns show that practically similar mineral combinations have been fractionated in almost all magmas. These minerals are not always found in the samples that represent the coarse-grained fraction so the phases probably have been enriched in the smaller grain-sized fractions or been fractionated during transport.

Comparison with Land-Based Data and Correlation

Marti et al. (1994) distinguished two main groups, the Upper and the Lower Group in the Las Cañadas caldera wall. The Lower Group (2–3.5 Ma) has not been studied in detail. The Upper Group was sep-

arated into three subunits within the 600-m-thick series exposed in the caldera wall from northeast to southwest: the Diego Hernandez (0.17–0.37 Ma), Guajara (0.65–0.85 Ma), and Ucanca Formations (1.2–1.6 Ma). These volcanic phases are postulated to be separated by periods of quiescence lasting between 0.3 and 0.4 Ma. Our data do not corroborate the alternation of volcanically active and inactive phases. Instead, the submarine tephra layers reflect volcanic activity throughout the past 3 m.y. (Fig. 2).

The correlation of individual ash layers from the proximal to the more distal sites as well as to DSDP Site 397 requires more detailed textural and chemical analyses of glass shards and phenocrystic minerals and has not been achieved in the present preliminary study. The problems in correlating ash layers between drill sites are mostly attributed to the missing parts of Hole 954A, whose ash layers should correlate with Hole 953.

DISCUSSION

Our data allow reconstruction of the chemical evolution of the Cañadas volcanic complex, as most analyzed glasses are fresh. The chemical composition of glasses changes with age from trachytic to phonolitic. These changes in composition of the magma cannot be explained by crystal fractionation. If the phonolitic magma were generated by crystal fractionation from a trachytic parent magma, then SiO_2 -rich phases such as alkali feldspar should be fractionated. This fractionation would not, however, result in the enrichment of alkalis, which we

Table 2. XRF analyses of pumice glass.

Hole:	953A	954A	954A	954A	954B	956A	956A	956A
Core, Section:	2H-4	4H-3	7H-4	9H-2	4R-2	9H-2	9H-3	11H-2
Interval (cm):	77-79	43-44	59-61	145-147	35-37	22-27	15-21	68-70
Depth (mbsf):	12.87	23.43	53.59	70.45	111.6	74.32	75.75	93.78
Age (Ma):	0.38	0.43	0.77	0.96	2.61	2.29	2.33	2.69
Major elements (wt%)								
SiO ₂	55.37	54.82	44.28	59.46	58.31	57.06	58.19	55.46
TiO ₂	0.56	0.57	3.65	0.63	0.42	0.58	0.51	0.89
Al ₂ O ₃	18.94	17.71	14.03	16.64	17.63	16.86	17.47	16.00
Fe ₂ O ₃	3.26	3.89	12.75	3.34	3.00	3.09	3.13	3.96
MnO	0.173	0.178	0.173	0.268	0.239	0.175	0.167	0.212
MgO	0.33	0.23	6.00	0.23	0.17	0.35	0.21	0.6
CaO	1.4	2.03	10.16	0.86	0.63	1.96	1.03	4.2
Na ₂ O	8.45	8.18	3.27	7.97	7.78	6.69	7.09	6.48
K ₂ O	5.47	5.33	1.53	5.2	5.35	5.24	5.43	4.46
P ₂ O ₅	0.111	0.063	0.673	0.062	0.044	0.077	0.067	0.155
SO ₃	0.196	1.059	0.065	0.192	0.204	0.333	0.49	0.289
H ₂ O+CO ₂	3.87	4.38	1.98	3.48	4.53	5.42	4.43	4.79
Total	98.35	98.69	98.86	98.55	98.5	98.08	98.46	97.71
Trace elements (ppm)								
Sc	2	8	26	5	4	5	6	2
V	25	27	214	<12	<12	<12	21	<12
Cr	<18	<18	241	<18	<18	<18	<18	<18
Co	7	<4	29	<4	15	<4	9	<4
Ni	18	20	102	14	17	14	22	18
Cu	19	60	72	18	24	16	13	16
Zn	164	125	125	160	152	114	112	138
Ga	38	33	18	32	34	32	32	29
As	18	22	<12	<12	<12	12	14	<12
Rb	188	165	24	153	157	155	157	113
Sr	120	88	947	27	29	149	107	269
Y	23	31	32	48	38	31	29	39
Zr	1117	1033	287	1156	1137	1040	1026	843
Nb	195	210	75	241	230	189	183	195
Mo	6	5	9	16	20	11	16	12
Ba	185	86	508	41	137	457	480	195
La	154	457	328	419	186	401	427	528
Ce	130	173	99	247	193	158	166	168
Pr	19	54	41	60	24	47	49	62
Nd	32	42	47	82	48	42	39	58
Sm	11	<6	10	16	9	11	<6	13
Pb	25	21	7	28	17	21	18	17
Th	42	33	<4	23	30	22	21	9
U	11	8	<6	<6	8	<6	8	<6

observed. Therefore, a change in composition of the mantle source and thus of the primitive mafic parent magmas from alkali basaltic to nephelinitic is postulated. A similar change from SiO₂-saturated to undersaturated derivative magmas between ~13.5 and 12 Ma on Gran Canaria from the Mogán to the Fataga Group volcanics has been observed (Schmincke and von Rad, 1979; Schmincke, 1982). In addition, this temporal change in source composition may indicate a general change of magma generation from the highly productive shield stage and high melting rates to a migration of the mantle source into the cooler marginal parts of the diapir that may have become increasingly mixed with lithospheric material (Hoernle and Schmincke, 1993).

Because submarine tephra differs mineralogically and geochemically from phonolithic lava flows and pyroclastic rocks on land, correlation remains difficult. Equivalent land deposited tephra is rarely exposed and covered by younger lava flows. Usually the mineral assemblages change during the sedimentation process. This is the reason why the glass and mineral chemistries are most useful for correlations. Because analyzed trace elements of the glasses are not distinctive, only the major elements can be used for a rough classification. Very few geochemical data, in particular of glasses, have been determined from the huge caldera wall. The mineral chemistry, especially the chemical differences in REEs of sphene between individual layers, may be helpful as a marker for correlating the submarine tephra with land deposits in the caldera wall. Depending on the frequency of magma mixing processes in the equivalent time period, Sample 157-953A-2H-4, 77–79 cm, would be easy to identify on land.

The submarine tephra records a continuous explosive volcanic activity of the trachytic and phonolithic Las Cañadas edifice between

3.8 and 0.3 Ma. The lack of tephra younger than 0.3 Ma roughly delimits the beginning of the less explosive activity of Pico Viejo and Pico de Teide growing from the base of the Las Cañadas caldera on Tenerife.

ACKNOWLEDGMENTS

We thank the Deutsche Forschungsgemeinschaft for financial support (Grants SCHM 250/43-3, 61-1). Part of the work was financed by grants from the European Commission. ICP-MS analyses were performed by C.D. Garbe-Schönberg (Geologisches Institut, Universität Kiel). The grain sizes <63 µm were determined on a laser particle analyzer by Takechi Kawahara (Earthquake Research Institute, Tokyo). Many thanks to Susanne Straub and Martin Streck for providing helpful advises. We also thank Petra Gloer, Jürgen Freitag (electron microprobe), Antje Merkau (X-ray fluorescence), and Alex Wülpers (core repository, Bremen) for technical help. We acknowledge James H. Wittke and Gordon Haxel for carefully reviewing the paper.

REFERENCES

- Ancochea, E., Fúster, J.M., Ibarrola, E., Cendrero, A., Coello, J., Hernán, F., Cantagrel, J.M., and Jamond, C., 1990. Volcanic evolution of the island of Tenerife (Canary Islands) in the light of new K-Ar data. *J. Volcanol. Geotherm. Res.*, 44:231–249.
- Coello, J., Cantagrel, J.-M., Hernán, F., Fúster, J.-M., Ibarrola, E., Ancochea, E., Casquet, C., Jamond, C., Díaz de Téran, J.-R., and Cendrero, A.,

1992. Evolution of the eastern volcanic ridge of the Canary Island based on new K-Ar data. *J. Volcanol. Geotherm. Res.*, 53:251–274.
- Dehn, J., Farrell, J.W., and Schmincke, H.-U., 1991. Neogene tephrochronology from Site 758 of the northern Ninetyeast Ridge: Indonesian Arc volcanism of the past 5 Ma. In Weissel, J., Peirce, J., Taylor, E., Alt, J., et al., *Proc. ODP, Sci. Results*, 121: College Station, TX (Ocean Drilling Program), 273–298.
- Fisher, R.V., and Schmincke, H.-U., 1984. *Pyroclastic Rocks*: New York (Springer-Verlag).
- Hoernle, K., and Schmincke, H.-U., 1993. The role of partial melting in the 15-Ma geochemical evolution of Gran Canaria: a blob model for the Canary Hotspot. *J. Petrol.*, 34:599–627.
- Marti, J., Mitjavila, J., and Villa, I., 1989. Stratigraphy and K-Ar ages of the Diego Hernández wall and their significance on the Las Cañadas Caldera Formation (Tenerife, Canary Islands). *Terra Nova*, 2:148–153.
- Marti, J., Mitjavila, J., and Araña, V., 1994. Stratigraphy, structure, age and origin of the Cañadas Caldera (Tenerife, Canary Islands). *Geol. Mag.*, 31:715–727.
- Oberti, R., Smith, D.C., Rossi, G., and Caucia, F., 1991. The crystal-chemistry of high-aluminium spenes. *Eur. J. Mineral.*, 3:777–792.
- Paterne, M., Guichard, F., and Labeyrie, J., 1988. Explosive activity of the south Italian volcanoes during the past 80,000 years as determined by marine tephrochronologie. *J. Volcanol. Geotherm. Res.*, 34:153–172.
- Schmincke, H.-U., 1982. Volcanic and chemical evolution of the Canary Islands. In von Rad, U., Hinz, K., Sarnthein, M., and Seibold, E. (Eds.), *Geology of the Northwest African Continental Margin*: Berlin (Springer), 273–306.
- Schmincke, H.-U., and von Rad, U., 1979. Neogene evolution of Canary Island volcanism inferred from ash layers and volcanoclastic sandstones of DSDP Site 397 (Leg 47A). In von Rad, U., Ryan, W.B.F., et al., *Init. Repts. DSDP*, 47 (Pt. 1): Washington (U.S. Govt. Printing Office), 703–725.
- Schmincke, H.-U., Weaver, P.P.E., Firth, J.V., et al., 1995. *Proc. ODP, Init. Repts.*, 157: College Station, TX (Ocean Drilling Program).
- Straub, S., 1995. Contrasting compositions of Mariana Trough fallout tephra and Mariana Island arc volcanics: a fractional crystallization link. *Bull. Volcanol.*, 57:403–421.
- Sun, S.-S., and McDonough, W.F., 1989. Chemical and isotopic systematics of oceanic basalts: implications for mantle composition and processes. In Saunders, A.D., and Norry, M.J. (Eds.), *Magmatism in the Ocean Basins*. Geol. Soc. Spec. Publ. London, 42:313–345.
- Wolff, A.J., 1985. Zonation, mixing and eruption of silica-undersaturated alkaline magma: a case study from Tenerife, Canary Islands. *Geol. Mag.*, 6:623–640.
- Wolff, J.A., Woerner, G., and Blake, S., 1990. Gradients in physical parameters in zoned felsic magma bodies: implications for evolution and eruptive withdrawal. *J. Volcanol. Geotherm. Res.*, 43:37–55.

Date of initial receipt: 3 July 1996

Date of acceptance: 6 January 1997

Ms 157SR-117

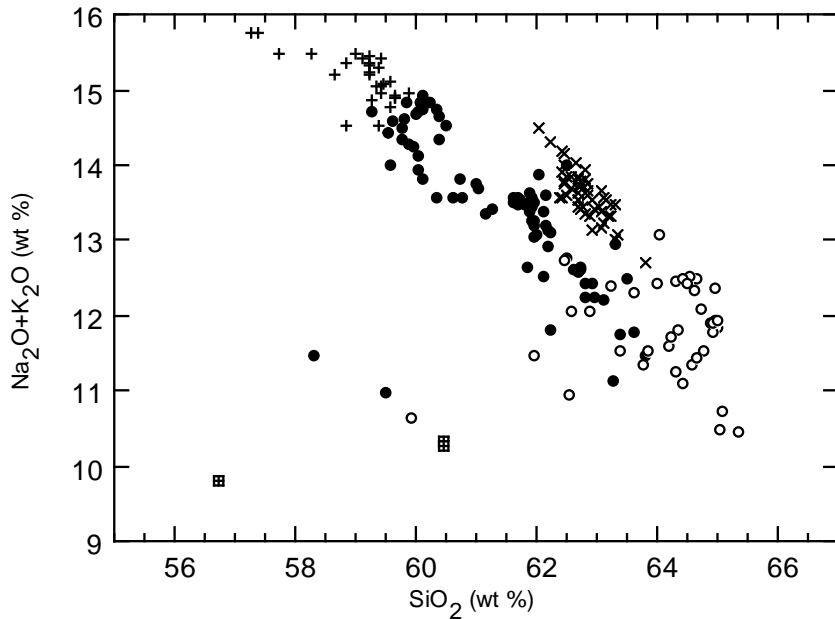
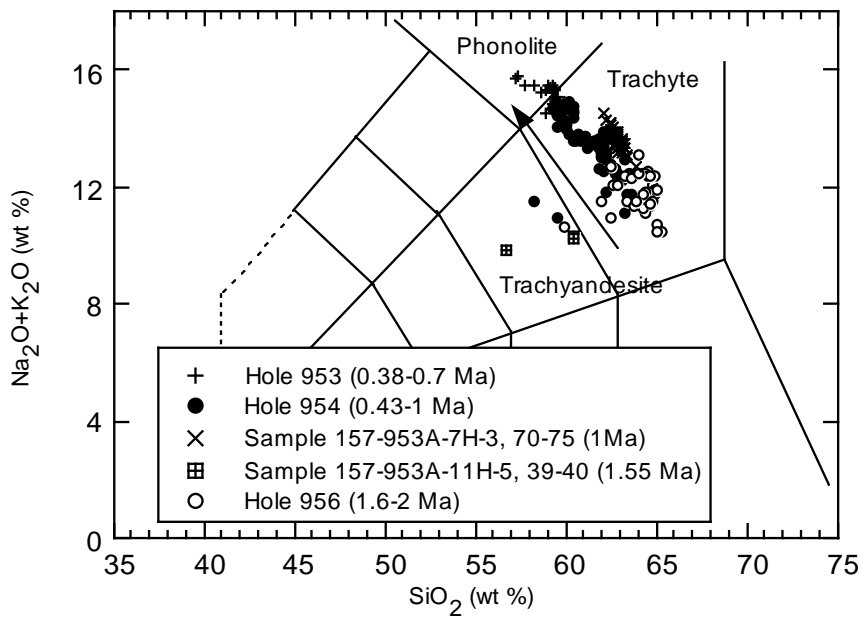


Figure 6. TAS diagram of electron microprobe analyses from pumice glasses, showing the evolution from trachytic to phonolitic composition with age (Site 956 samples are 1.6–2 Ma, Site 954 0.43–1 Ma, and those from Site 953 0.38–1.6 Ma). The compositions are normalized to 100%. The pumice of Sample 157-953A-7H-3, 70–75 cm, containing no phenocrysts, follows the trend, but covers a wide range in composition.

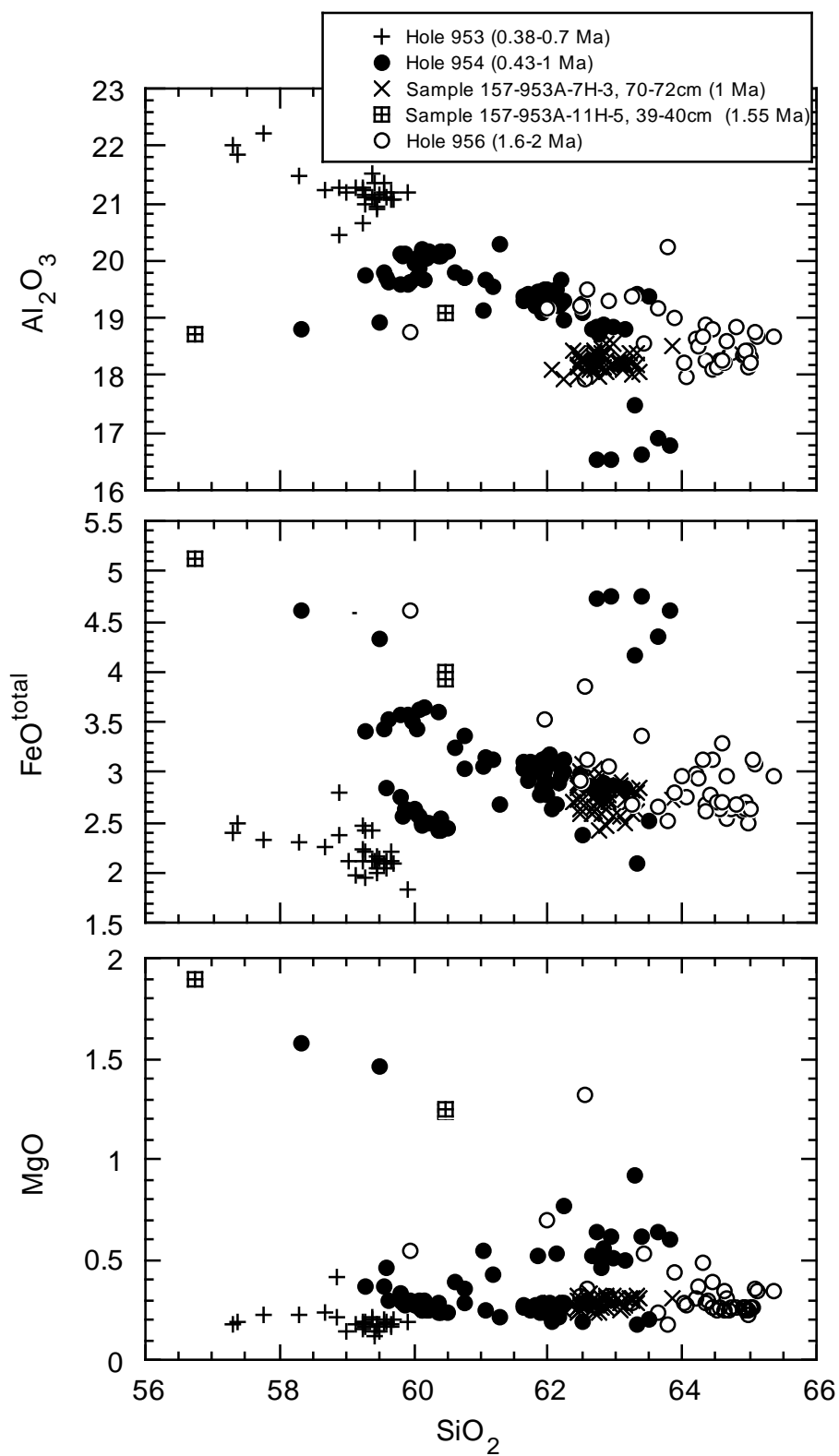


Figure 7. Variation diagrams (MgO , $\text{FeO}^{\text{total}}$, and Al_2O_3 vs. SiO_2) of pumice glass from tephra layers from Sites 953, 954, and 956.

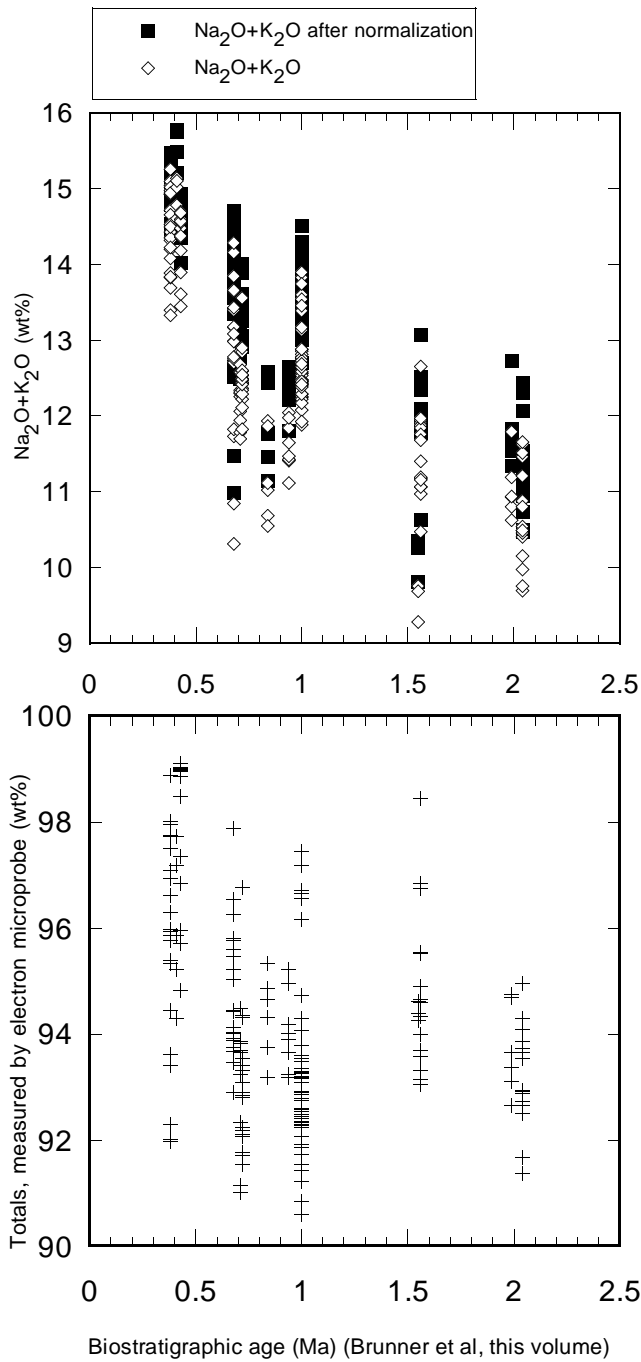


Figure 8. The totals from electron microprobe analyses of the pumice glasses show no significant dependence on age (lower plot). Volatile-free normalization does not therefore influence the trends (Na₂O + K₂O; upper plot).

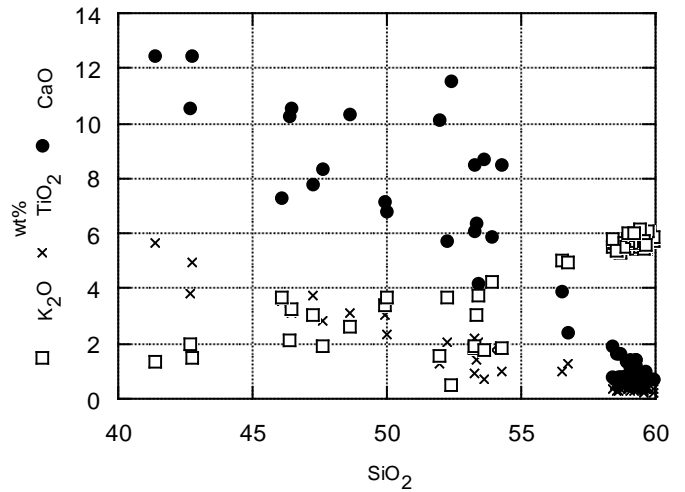


Figure 9. CaO, K₂O, and TiO₂ vs. SiO₂ measured by electron microprobe of pumice glass from Sample 157-953A-2H-4, 77-79 cm, indicating magma mixing.

Table 3. Representative data of glass shards (pumice) and minerals.

Hole, core, section:	954A-6H-5	953A-2H-4	956A-7H-6	954A-7H-4									953A-2H-5	954A-6H-5	956A-7H-CC							
Interval (cm):	71-73	77-79	70-76	59-61									149-150	71-73	7-9							
Depth (mbsf):	45.71	12.87	61.80	53.59									15.09	45.71	63.23							
Mineral:	Titanite	Kaersutite	Pyroxene	Pyroxene	Hauyne	Sodalite	Nepheline	Pumice	Pumice	Pumice	Pumice	Pumice	Pumice	Pumice								
Points/minerals:	128/5	30/5	36/6	33/4	18/1	34/3	10/2	5/1	4/1	44/9	97/9											
	Stdev.	Stdev.	Stdev.	Stdev.	Stdev.	Stdev.	Stdev.	Stdev.	Stdev.	Stdev.	Stdev.	Stdev.	Stdev.	Stdev.	Stdev.							
SiO ₂	28.99	0.22	37.89	0.40	47.53	1.01	47.91	1.59	34.27	0.43	37.19	0.20	44.922	0.365	57.02	0.52	54.93	1.27	57.27	1.21	59.67	0.68
TiO ₂	34.50	0.37	6.79	0.29	2.26	0.47	1.93	0.64	0.05	0.04	0.03	0.04	0.034	0.037	0.47	0.08	0.44	0.09	0.70	0.11	0.61	0.12
Al ₂ O ₃	0.69	0.09	14.11	0.39	5.71	0.92	6.18	1.05	27.80	0.28	30.15	0.34	33.114	0.249	20.63	0.17	21.11	0.21	18.63	0.25	17.69	0.55
FeO ^{total}	2.02	0.10	10.73	0.34					0.25	0.06	0.34	0.06	0.577	0.045	2.19	0.22	2.30	0.07	3.07	0.17	2.82	0.19
FeO					3.99	0.36	3.50	0.75														
Fe ₂ O ₃					3.68	0.98	3.68	0.60														
MnO	0.22	0.03	0.13	0.05	0.21	0.15	0.11	0.04	0.02	0.02	0.02	0.03	0.013	0.013	0.16	0.07	0.22	0.05	0.28	0.06	0.24	0.05
MgO	0.00	0.00	12.82	0.22	13.16	0.75	14.03	1.19	0.00	0.01	0.01	0.01	0.013	0.013	0.23	0.03	0.17	0.02	0.37	0.04	0.32	0.10
CaO	25.58	0.25	12.40	0.15	22.42	0.39	21.62	0.70	8.00	0.14	0.37	0.16	0.779	0.178	0.91	0.04	0.75	0.03	0.60	0.05	0.61	0.17
BaO			0.17	0.06									0.041	0.044								
Na ₂ O	0.28	0.04	2.56	0.07	0.60	0.15	0.54	0.07	16.21	0.29	23.16	0.20	16.791	0.142	8.89	0.10	9.57	0.56	7.99	0.55	6.25	0.50
K ₂ O	0.01	0.02	0.88	0.06	0.01	0.00	0.00	0.01	0.89	0.13	1.77	0.14	3.442	0.156	5.89	0.21	5.54	0.16	4.98	0.15	4.55	0.21
P ₂ O ₅			0.09	0.04											0.09	0.03	0.06	0.03	0.07	0.03	0.08	0.04
F	0.21	0.03	0.16	0.02					0.04	0.03	0.03	0.03	0.057	0.037	0.21	0.11	0.23	0.05	0.22	0.05	0.16	0.03
Cl			0.02	0.01					0.52	0.02	5.37	0.10	0.010	0.010	0.42	0.06	0.52	0.07	0.31	0.07	0.28	0.07
S			0.05	0.03					8.44	0.21	0.38	0.09			0.04	0.04	0.05	0.05	0.10	0.03	0.10	0.06
Cr ₂ O ₃					0.06	0.05	0.15	0.12														
NiO					0.04	0.02	0.02	0.02														
ZrO ₂	0.64	0.31																				
Nd ₂ O ₃	0.79	0.10																				
V ₂ O ₅	1.13	0.04																				
La ₂ O ₃	0.52	0.07																				
Ce ₂ O ₃	1.56	0.12																				
Total	97.15	0.40	98.82	0.41	99.63	0.22	99.68	0.31	96.49	0.33	98.83	0.61	99.792	0.400	97.17	0.80	95.88	2.13	94.59	1.50	93.39	0.96
Fe ³ /Fe ²					1.068	0.384	0.896	0.315														
Mg/Mg+Fe _{total}					0.763	0.033	0.784	0.032														
EN					43.623	2.509	47.245	2.856														
FS					11.080	2.011	10.769	1.700														
WO					45.298	0.895	41.987	2.026														

Notes: Stdev. = standard deviation. All values in weight percent.

Table 4. ICP-MS analyses of pumice glasses.

Hole, core, section:	954A-9H-4	954A-6H-5	953A-2H-5
Interval (cm):	33-34	71-73	149-150
Depth (mbsf):	72.33	45.71	15.09
Trace elements (ppm)			
Sc	1.77	0.95	1.57
Cr	19.7	10.1	11.2
Co	3.20	0.80	1.72
Ni	7.83	2.11	
Cu	10.7	5.60	7.80
Zn	157.2	206.7	153.2
Ga	35.7	37.8	41.8
Rb	232.6	161.9	282.8
Cs	3.49	2.05	4.62
Sr	323.9	25.9	79.2
Y	31.2	69.9	33.2
Zr	1436	1300	1969
Nb	236.4	360.9	304.4
Ba	315.6	150.8	130.2
La	142.1	219.0	138.4
Ce	185.5	379.5	182.3
Pr	14.4	37.0	13.9
Nd	38.1	113.2	35.9
Sm	5.12	17.7	5.08
Eu	1.23	3.75	0.98
Gd	4.60	14.24	4.57
Tb	0.68	2.12	0.70
Dy	4.09	11.8	4.40
Ho	0.88	2.28	0.97
Er	2.96	6.56	3.42
Tm	0.50	0.92	0.60
Yb	3.89	6.07	4.67
Lu	0.63	0.85	0.75
Th	38.0	28.9	55.9
Ta	7.56	18.6	10.3
Hf	25.7	25.5	35.4
U	9.61	6.94	15.2
Pb	23.0	16.1	29.2

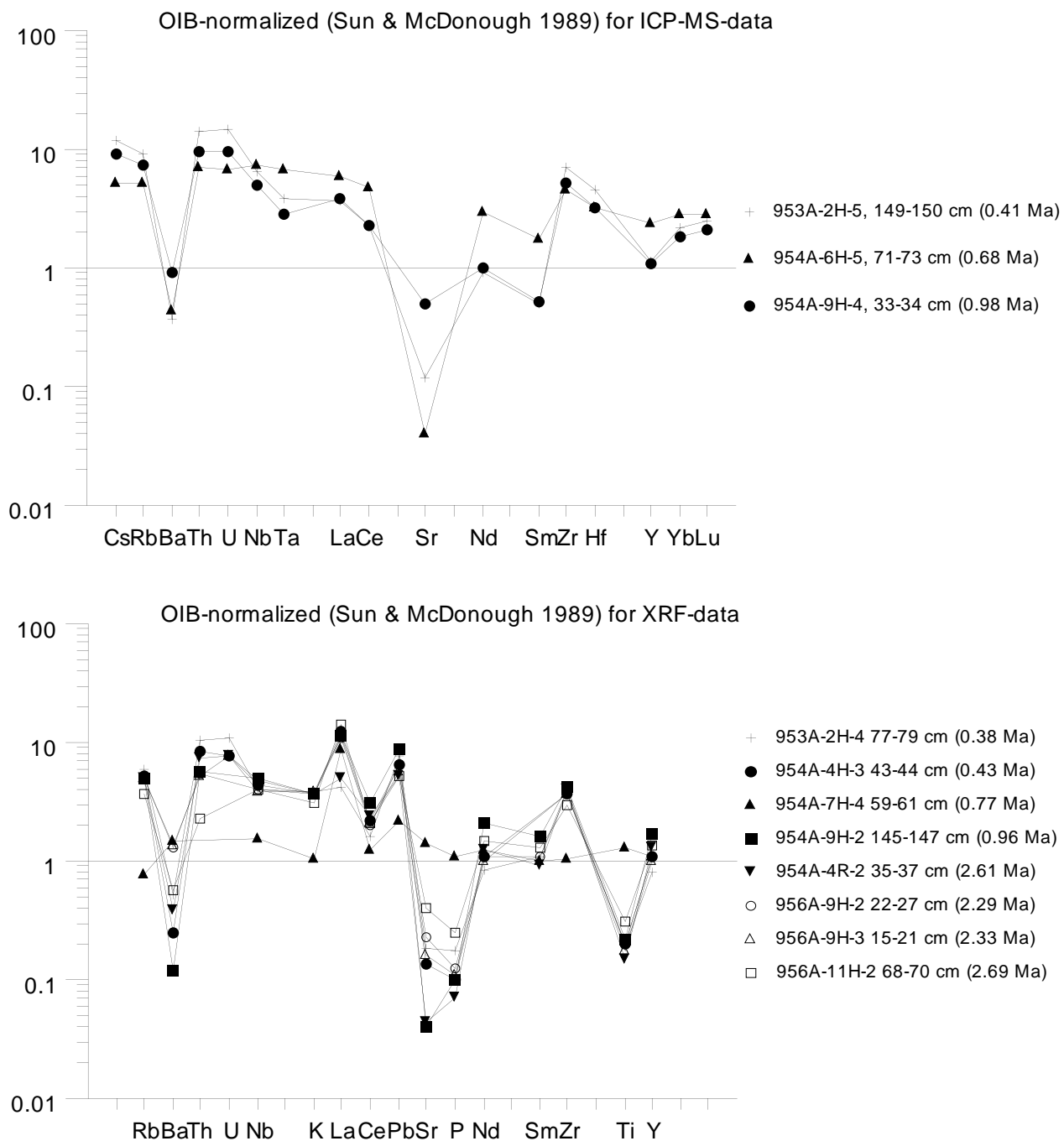


Figure 10. Trace element concentrations of several pumice glasses and tephra of basaltic composition (Sample 157-954A-7H-4, 59–61 cm; 0.77 Ma) analyzed by XRF. Three pumice samples were measured with ICP-MS. The data are normalized against OIB (Sun and McDonough, 1989).